

Study of Sodium-ion Battery Based on Sodium Vanadium Phosphate and Sodium Titanate at Low Temperatures

Tatiana Kulova^{1,4,*}, Alexander Skundin^{1,4}, Andrew Chekannikov², Svetlana Novikova³,
Irina Stenina³, Yulia Kudryashova^{1,4}, Grigorii Sinenko⁵

¹ A.N. Frumkin Institute of Physical Chemistry and Electrochemistry of the Russian Academy of Sciences, 31-4, Leninskii Prospect, 119071, Moscow, Russia

² Skolkovsky Institute of Science and Technology, 121205, 3, ul. Nobel, Moscow, Russia

³ N.S. Kurnakov Institute of General and Inorganic Chemistry of the Russian Academy of Sciences, 119991, 31, Leninskii Prospect, Moscow, Russia

⁴ National Research University "MEI", 111250, 14, ul. Krasnokazarmennaya, Moscow, Russia

⁵ Lomonosov Moscow State University, 119991, 1, Leninskie Gory, Moscow, Russia

*E-mail: tkulova@mail.ru

Received: 13 October 2018 / Accepted: 19 November 2018 / Published: 5 January 2019

The purpose of this work was to study the performance of a sodium-ion battery based on the sodium vanadium phosphate /sodium titanate in the temperature range from +20 to –45 °C. To achieve this goal the methods of galvanostatic cycling and pulse chronopotentiometry were used. The performance of sodium-ion battery at low temperatures was found to be limited by the functioning of the negative electrode based on sodium titanate, which remains operational only at temperatures not less than –35 °C. The positive electrode based on sodium vanadium phosphate is efficient at temperatures down to –45 °C. The activation energy of sodium diffusion in the sodium vanadium phosphate and the sodium titanate is about 42 and 70 kJ / mol, respectively.

Keywords: Sodium-ion battery; Low temperatures; Activation energy of diffusion

1. INTRODUCTION

One of the candidates for the next generation of secondary power sources is the sodium-ion battery (SIB). Despite the lower specific energy and power compared to lithium-ion batteries (LIBs), SIBs will be characterized by a lower cost of stored energy. This means that SIBs are quite competitive with LIBs. At present, various functional materials have been developed for negative and positive electrodes of SIB capable of operating over a wide current range, but the question of their functioning at different temperatures (especially low ones) is still open. The operation of the sodium-ion battery at low

temperatures can be limited by both the operation of one of the electrodes and the conductivity of the electrolyte.

Literature data on the effect of low temperatures on the reversible insertion of sodium into functional electrode materials of the sodium-ion battery are few in numbers. For example, the authors of [1] describe processes in materials based on hard carbon (a negative electrode of SIB), while the temperature range is limited by a temperature of minus 15 °C. For the positive electrode, Guo *et al.* [2] have reported the results of a study of a material based on $\text{Na}_3\text{V}_2(\text{PO}_4)_2\text{O}_2\text{F}$ in the temperature range from +25 to -25 °C (the discharge capacity decreased from 130 to 90 mAh g⁻¹ when the temperature was lowered from +25 to -25 °C). The authors of [3] when discussing the possibilities of SIB practical applications presented some results of testing electrode based on $\text{Na}_{1.92}\text{Fe}(\text{CN})_6$ in the temperature range from +20 to -40 °C. Such a cathode was shown to be functionable at the temperature as low as -40 °C, capacity loss being a mere 30% from nominal value. A superior cycling was obtained for MXene/SnS₂ electrodes [4], in particular, a reversible capacity of 120 mAh g⁻¹ after 125 cycles at 0 °C has been reached. In [5] a Sb@graphene composite with a lamellar structure demonstrated good low-temperature properties (e.g., 506.6 and 472.5 mAh g⁻¹ at 25 and 50 mA g⁻¹ at -20 °C, respectively) as anode of SIB. The authors of [6] have reported the study of carbon-coated $\text{Na}_3\text{V}_2(\text{PO}_4)_3$ in a wide temperature range (*i.e.*, from -20 to 55 °C). Even at a temperature of -20 °C, the $\text{Na}_3\text{V}_2(\text{PO}_4)_3$ cathode can still maintain a discharge capacity of 91.3 mA h g⁻¹ or 85.2% of the room performance at 10C. These excellent wide-temperature accomplishments can be ascribed to fast three-dimensional Na⁺ hopping transportation mechanism in the NASICON structure. The finding in this work offers a promising strategy to address the long-standing inherent wide-temperature issues of rechargeable batteries and extends the potential application of sodium ion batteries. The authors [7] have presented a comparative study of spirally wound full cells consisting of $\text{Li}_{0.1}\text{Na}_{0.7}\text{Co}_{0.5}\text{Mn}_{0.5}\text{O}_2$ (or $\text{Li}_{0.8}\text{Co}_{0.5}\text{Mn}_{0.5}\text{O}_2$) and hard carbon and report that the power of sodium-ion battery at -30 °C is ~21% higher than that of lithium-ion battery.

The novelty of this article is that it contains the results of a study of the behavior of positive electrode based on sodium vanadium phosphate, negative electrode based on sodium titanate, as well as a full cell based on these functional materials in the temperature range from +20 to -45 °C.

2. EXPERIMENTAL

2.1 Synthesis of positive electrode material of the sodium-ion battery

The composite of sodium vanadium phosphate with carbon $\text{Na}_3\text{V}_2(\text{PO}_4)_3@\text{C}$ was chosen as the material of the positive electrode of SIB. $\text{Na}_3\text{V}_2(\text{PO}_4)_3@\text{C}$ composites were prepared using the modified Pechini method according to the procedure described in [8]. V_2O_5 , oxalic acid, NaNO_3 , $\text{NH}_4\text{H}_2\text{PO}_4$ and citric acid were mixed in a molar ratio of 1: 6: 3: 3: 2 and placed in a beaker with water and ethylene glycol mixed in a 3:7 by volume ratio. The mixture was kept under heating (50-80 °C) and stirring until the solids were completely dissolved. The solution was heated to 300 °C and held for 2 hours. The residue was ground in a planetary mill (800 rpm, 8 h) and annealed in an Ar atmosphere for 10 hours at 600 °C and for 2 hours at 800 °C.

2.2 Synthesis of negative electrode material of the sodium-ion battery

A composite of sodium titanate with carbon ($\text{Na}_2\text{Ti}_3\text{O}_7@\text{C}$) was chosen as the material of the negative electrode of SIB. Sodium titanate was prepared by a citric method. The stoichiometric amounts of tetrabutyl titanate (99+%, Alfa Aesar) and anhydrous sodium carbonate (ACS reagent $\geq 99.5\%$, Sigma-Aldrich) were dissolved in the mixture of nitric acid and ethanol (1:10, v/v). Then citric acid water solution was added. The molar ratio of citric acid to titanium was 4:1. The mixture was then heat treated at 95 and 250 °C, grounded in an agate mortar and annealed at 800 °C for 5 h.

2.3 Materials characterization

The phase composition of the obtained samples was characterized using a Rigaku D / MAX 2200 diffractometer, $\text{CuK}\alpha$ radiation in the range 10-60 ° 2θ . The size of the coherent scattering regions (CSR) was calculated from the broadening of the peaks on the diffractograms, using the Scherrer formula [9]:

$$d = \frac{k\lambda}{\sqrt{B^2 - b^2} \cos\theta} , \quad (1)$$

where d is the crystallite size, λ is the wavelength, θ is the diffraction angle, k is 0.9 is the Scherrer constant, B is the width of the peak at half-height, and b is the width of the standard line. The instrumental broadening was determined using the LaB_6 SRM 660a standard. The carbon content of the composites was determined using the Euroa 3000 CHNS analyzer. The microstructure of the samples was analyzed using a scanning electron microscope Carl Zeiss NVision 40 equipped with an energy-dispersive X-ray (EDX) analyzer operating at an accelerating voltage of 15 kV.

2.4 Electrochemical study

The active masses of the positive (80% $\text{Na}_3\text{V}_2(\text{PO}_4)_3@\text{C}$, 15% carbon black (Timcal), 5% PVDF (Sigma-Aldrich) dissolved in NMP (Sigma-Aldrich)) and the negative (80% $\text{Na}_2\text{Ti}_3\text{O}_7@\text{C}$, 15% carbon black (Timcal), 5% PVDF (Sigma-Aldrich), dissolved in NMP (Sigma-Aldrich)) electrodes were applied to an aluminum foil substrate using a doctor blade. Then the electrodes were dried to constant weight in a drying oven at a temperature of 90 °C, pressed at a pressure of 1 ton cm^{-2} , and further dried under vacuum at 120 °C for 12 hours. The size of the electrodes was 2.25 cm^2 . The content of active substances on the substrate was 2–2.5 mg cm^{-2} of $\text{Na}_2\text{Ti}_3\text{O}_7@\text{C}$ and 5–7 mg cm^{-2} of $\text{Na}_3\text{V}_2(\text{PO}_4)_3@\text{C}$.

As the electrolyte, 1 M NaClO_4 in a mixture of ethylene carbonate and propylene carbonate (1:1, v/v) was used. The water content of the electrolyte, measured by the method of coulometric titration according to Fisher (917 Ti-Touch, Switzerland), did not exceed 20 ppm.

For the investigation of $\text{Na}_3\text{V}_2(\text{PO}_4)_3@\text{C}$ and $\text{Na}_2\text{Ti}_3\text{O}_7@\text{C}$, sealed three-electrode electrochemical cells (half-cells) were assembled. The auxiliary electrode and the reference electrode were made from sodium metal rolled on a stainless steel substrate.

A pouch full cell containing a positive electrode ($\text{Na}_3\text{V}_2(\text{PO}_4)_3@\text{C}$) and a negative electrode ($\text{Na}_2\text{Ti}_3\text{O}_7@\text{C}$) was assembled to study the operation of the sodium-ion battery model. As the separator, nonwoven polypropylene with a thickness of 15 μm (NGO UFIM, Russia) was used. The cells were assembled in a glove box with a dry argon atmosphere (JSC "Spectroscopic systems", Russia). The water and oxygen content in the box did not exceed 0.1 and 1 ppm, respectively. Galvanostatic cycling of electrodes was carried out at a current density of 20 mA g^{-1} of active substance. Cycling of the sodium-ion battery was carried out with a current of 0.086 mA, which corresponded to a current density of 20 mA g^{-1} of $\text{Na}_2\text{Ti}_3\text{O}_7@\text{C}$ and 10 mA g^{-1} of $\text{Na}_3\text{V}_2(\text{PO}_4)_3@\text{C}$. The mass ratio of $\text{Na}_3\text{V}_2(\text{PO}_4)_3@\text{C}$: $\text{Na}_2\text{Ti}_3\text{O}_7@\text{C}$ was 1: 2, to eliminate the irreversible capacity of sodium titanate in the first cycle. Studies of reversible sodium insertion into $\text{Na}_3\text{V}_2(\text{PO}_4)_3@\text{C}$ and $\text{Na}_2\text{Ti}_3\text{O}_7@\text{C}$ were conducted at temperatures of +20, -15, -20, -25, -30, -35, -40 and -45 $^\circ\text{C}$. The freezing point of the electrolyte 1 M NaClO_4 in the mixture of propylene carbonate – ethylene carbonate (1:1) is minus 80 $^\circ\text{C}$.

The pulse chronopotentiograms of electrodes based on $\text{Na}_3\text{V}_2(\text{PO}_4)_3@\text{C}$ and $\text{Na}_2\text{Ti}_3\text{O}_7@\text{C}$ were recorded at switching current (current densities from 5 to 400 mA g^{-1}) at temperatures of +20, -15, -25, -35, -45 $^\circ\text{C}$. The pulse duration was 25 s.

Electrochemical testing was carried out in galvanostatic mode with a charge-discharge galvanostat (Neware, China). The chronopotentiograms were recorded with using of potentiostat (Elins-8P, Russia). A cold-heat chamber (KTKh-65+165, Russia) to carry out low-temperature tests was used.

3. RESULTS AND DISCUSSION

3.1. XRD analysis and electron microscopy of $\text{Na}_3\text{V}_2(\text{PO}_4)_3@\text{C}$

According to XRD data the obtained sodium vanadium phosphate has the structure of NASICON rhombohedral modification (stretch $R\bar{3}c$) and does not contain impurity phases. The parameters of the unit cell are "a" = 8.731 ± 0.003 , "c" = 21.831 ± 0.001 . The size of the CSR is ~ 40 nm.

The carbon included in the $\text{Na}_3\text{V}_2(\text{PO}_4)_3@\text{C}$ is X-ray amorphous. The carbon content in the $\text{Na}_3\text{V}_2(\text{PO}_4)_3@\text{C}$, according to elemental analysis, was 8.9% by weight. The ratio of the element's Na:V:P according to X-ray spectral analysis corresponds to the initial loading.

According to the SEM data, micrographs of $\text{Na}_3\text{V}_2(\text{PO}_4)_3@\text{C}$ exhibit agglomerates measuring 200 nm to several microns with an average value of ~ 2 μm (Fig. 1a).

3.2. XRD analysis and electron microscopy of $\text{Na}_2\text{Ti}_3\text{O}_7@\text{C}$

According to XRD data, the refined parameters of the lattice of the sodium titanate are $a = 9.126 \pm 0.002$ \AA , $b = 3.7978 \pm 0.0007$ \AA , $c = 8.571 \pm 0.002$ \AA , $\beta = 101.60 \pm 0.002$ $^\circ$ (monoclinic syngony, space group P21/m). The values of the size of the CSR of sodium titanate calculated from the Debye-Scherrer formula were 595 and 425 nm. The SEM images of the sodium titanate samples under study show aggregates of particles having a layered morphology (Fig. 1b). Due to the high synthesis temperature, the size of the aggregates of the original $\text{Na}_2\text{Ti}_3\text{O}_7$ was sufficiently large (1 μm or more).

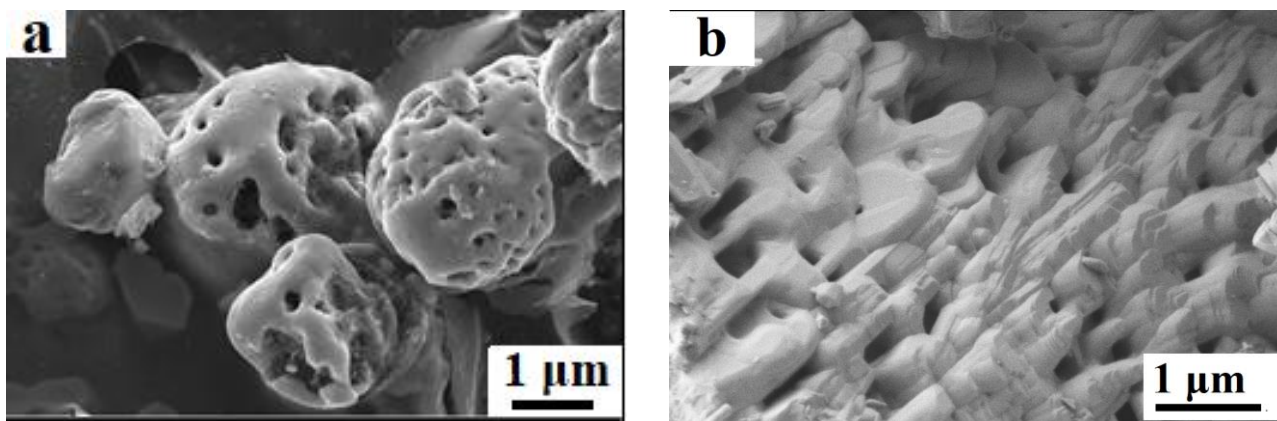


Figure 1. SEM images of $\text{Na}_3\text{V}_2(\text{PO}_4)_3@\text{C}$ (a) and $\text{Na}_2\text{Ti}_3\text{O}_7@\text{C}$ (b)

3.3 Results of electrochemical studies

The charge and discharge curves of electrodes based on $\text{Na}_3\text{V}_2(\text{PO}_4)_3@\text{C}$ and $\text{Na}_2\text{Ti}_3\text{O}_7@\text{C}$ are shown in Figure 2. Curves at temperature of 20 °C are typical for sodium vanadium phosphate [10, 11] and sodium titanate [12].

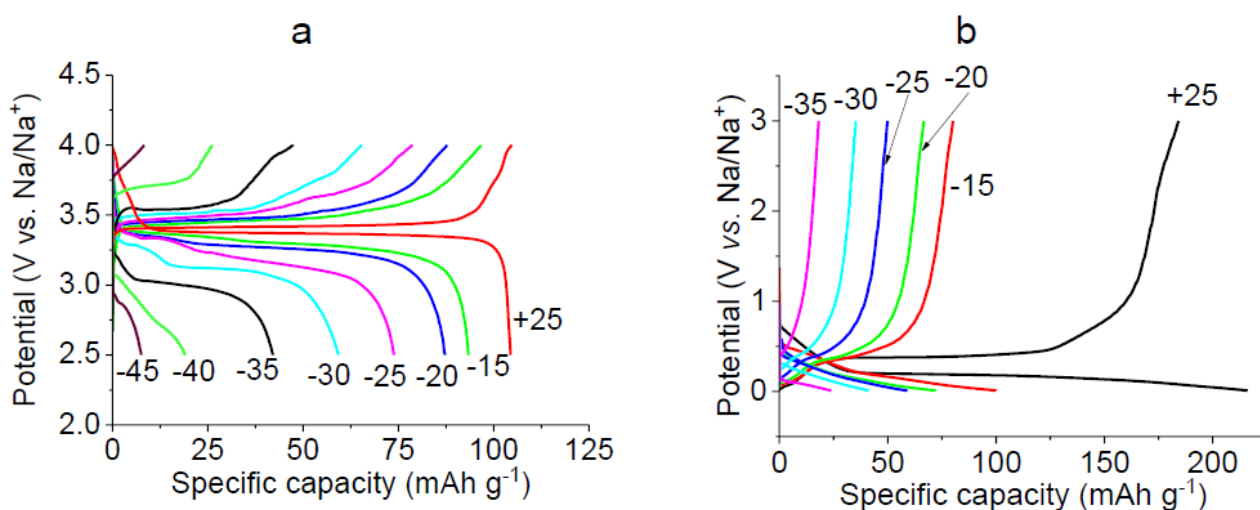


Figure 2. Charge and discharge curves at different temperatures for $\text{Na}_3\text{V}_2(\text{PO}_4)_3@\text{C}$ (a) and $\text{Na}_2\text{Ti}_3\text{O}_7@\text{C}$ (b). The current density of 20 mA g^{-1} of active substance. The operating temperatures (°C) are shown in the figures.

It was mentioned above that the freezing point of the electrolyte used (1M NaClO_4 in the PC-EC mixture (1:1, v/v)) is about -80 °C. This means that the reversible insertion of sodium into the materials of the positive and the negative electrodes at low temperatures should not be limited by the migration of ions in the electrolyte. An analysis of the charge-discharge curves depicted in Figure 2a shows that a decrease in operating temperature leads to a decrease in the specific capacity of $\text{Na}_3\text{V}_2(\text{PO}_4)_3@\text{C}$ and $\text{Na}_2\text{Ti}_3\text{O}_7@\text{C}$. In so doing it was found that $\text{Na}_3\text{V}_2(\text{PO}_4)_3@\text{C}$ is capable of

operating at temperatures up to minus 45 °C, while $\text{Na}_2\text{Ti}_3\text{O}_7@\text{C}$ remains operable at temperatures down to minus 35 °C only. Decreasing the operating temperature leads to a change in the shape of the charge and discharge curves and an increase in the polarization. Clear charge and discharge plateaus, corresponding to the two-phase mechanism of insertion-extraction of sodium, are transformed into inclined plateaus. Furthermore, for $\text{Na}_3\text{V}_2(\text{PO}_4)_3@\text{C}$ at temperatures minus 25 and minus 30 °C two charge-discharge plateaus (instead of one) are registered.

Data on testing the sodium-ion battery based on $\text{Na}_3\text{V}_2(\text{PO}_4)_3@\text{C}$ and $\text{Na}_2\text{Ti}_3\text{O}_7@\text{C}$ (full cell) indicate that the temperature dependence of battery capacity is stronger than for individual electrodes (Fig. 3a). In particular, the battery did not work at a temperature below minus 30 °C, while the electrodes tested in half cells operate at lower temperatures.

The dependencies of the relative discharge capacity (Q_d/Q_d^{20}) on the temperature (Figure 3b) for $\text{Na}_2\text{Ti}_3\text{O}_7@\text{C}$ and the full cell of the $\text{Na}_3\text{V}_2(\text{PO}_4)_3@\text{C}-\text{Na}_2\text{Ti}_3\text{O}_7@\text{C}$ system are practically linear and can be represented by the empirical equation:

$$Q_d/Q_d^{20} = 0.65 + kt, \quad (2)$$

where Q_d is discharge capacity at the appropriate temperature, Q_d^{20} - discharge capacity at a temperature of 20 °C.

The values of coefficient k in formula (2) are 0.015 and 0.016 for $\text{Na}_2\text{Ti}_3\text{O}_7@\text{C}$ -electrode and full-cell, respectively.

For $\text{Na}_3\text{V}_2(\text{PO}_4)_3@\text{C}$, a more complicated dependence of the discharge capacity on temperature was obtained. This relationship contains two linear sections. The first section in the temperature range from 20 °C to minus 15 °C can be described by equation

$$Q_d/Q_d^{20} = 0.92 + 0.0032t. \quad (3)$$

The second section in the temperature range from minus 15 to minus 45 °C is described by equation

$$Q_d/Q_d^{20} = 1.4 + 0.029t. \quad (4)$$

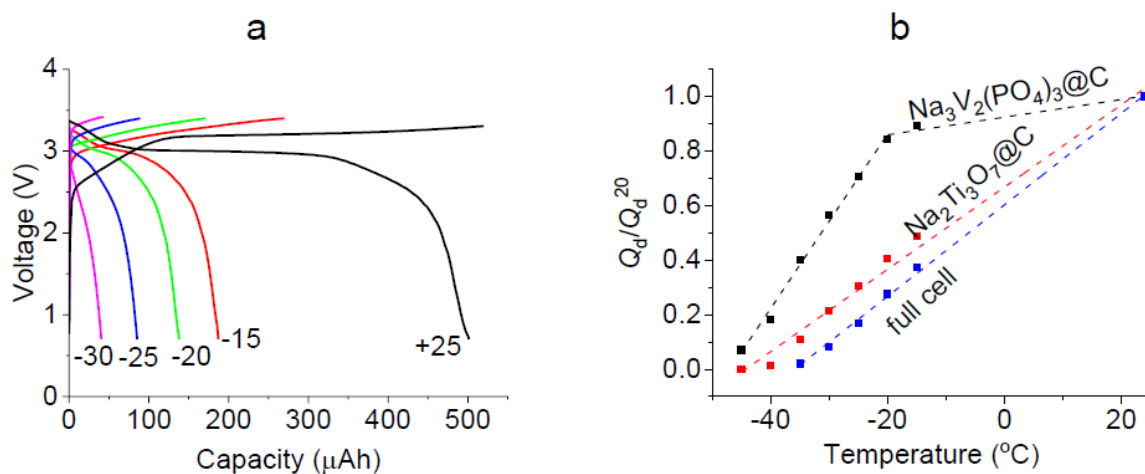


Figure 3. Charge and discharge curves at different temperatures of the full-cell based on $\text{Na}_3\text{V}_2(\text{PO}_4)_3@\text{C}-\text{Na}_2\text{Ti}_3\text{O}_7@\text{C}$ system; the temperatures (°C) are shown in the figure (a). Temperature dependences of the relative discharge capacity of $\text{Na}_3\text{V}_2(\text{PO}_4)_3@\text{C}$, $\text{Na}_2\text{Ti}_3\text{O}_7@\text{C}$ and the full cell (b)

To determine the reasons for such a strong difference in the electrochemical behavior of $\text{Na}_2\text{Ti}_3\text{O}_7@\text{C}$ and $\text{Na}_3\text{V}_2(\text{PO}_4)_3@\text{C}$ at low temperatures, the pulse chronopotentiograms of these electrodes were registered at temperatures of +20, -15, -25, -35, and -45 °C.

Cathodic pulse chronopotentiograms were recorded for the $\text{Na}_3\text{V}_2(\text{PO}_4)_3@\text{C}$ and the anodic ones were registered for $\text{Na}_2\text{Ti}_3\text{O}_7@\text{C}$ which corresponded to the processes at positive and negative electrodes at the sodium-ion battery discharge. Figure 4 shows the pulse chronopotentiograms in the diffusion coordinates potential (E) vs. square root from time ($\tau^{1/2}$) corresponding to different current densities at temperatures of +20, -15 and -35 °C at the equal degree of sodium intercalation. It is seen that the initial sections of the galvanostatic chronopotentiograms were linearized in these coordinates.

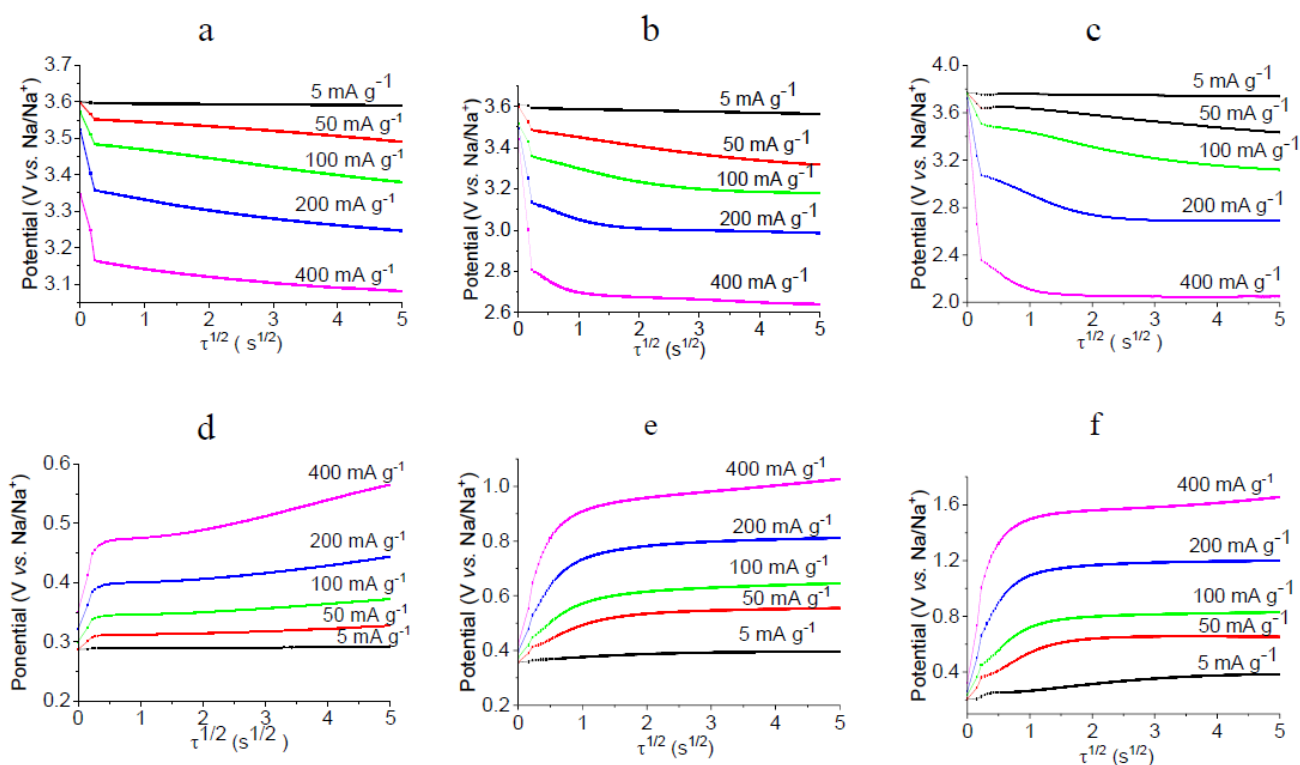


Figure 4. The chronopotentiograms of $\text{Na}_3\text{V}_2(\text{PO}_4)_3@\text{C}$ (a, b, c) and $\text{Na}_2\text{Ti}_3\text{O}_7@\text{C}$ (d, e, f) at temperatures of +20 (a, d), -15 (b, e) and -35 (c, f) °C at different current densities.

Figure 5 shows the dependence of $dE/d(\tau^{1/2})$ on the current density at different temperatures for $\text{Na}_3\text{V}_2(\text{PO}_4)_3@\text{C}$ and $\text{Na}_2\text{Ti}_3\text{O}_7@\text{C}$. It can be seen from the figure that all these dependences are linear and pass through origin. A decrease in operating temperature leads to an increase in the slope of the dependences $dE/d(\tau^{1/2})$ on the current density.

The true surface area of $\text{Na}_3\text{V}_2(\text{PO}_4)_3@\text{C}$ and $\text{Na}_2\text{Ti}_3\text{O}_7@\text{C}$ can be calculated by the formula:

$$S=3m/\rho R, \quad (5)$$

where m is the mass of the active material, ρ is the density of the active substance, and R is the radius of one particle. The density of the $\text{Na}_3\text{V}_2(\text{PO}_4)_3@C$ was assumed to be 2 g cm^{-3} , the $\text{Na}_2\text{Ti}_3\text{O}_7@C$ density was 3.195 g cm^{-3} .

Thus, the true surface area of the electrode based on $\text{Na}_3\text{V}_2(\text{PO}_4)_3@C$ can be estimated to be 112 cm^2 (agglomerates about $2 \mu\text{m}$). The true surface area of the electrode based on $\text{Na}_2\text{Ti}_3\text{O}_7@C$ can be estimated to be 42 cm^2 (agglomerates $1 \mu\text{m}$).

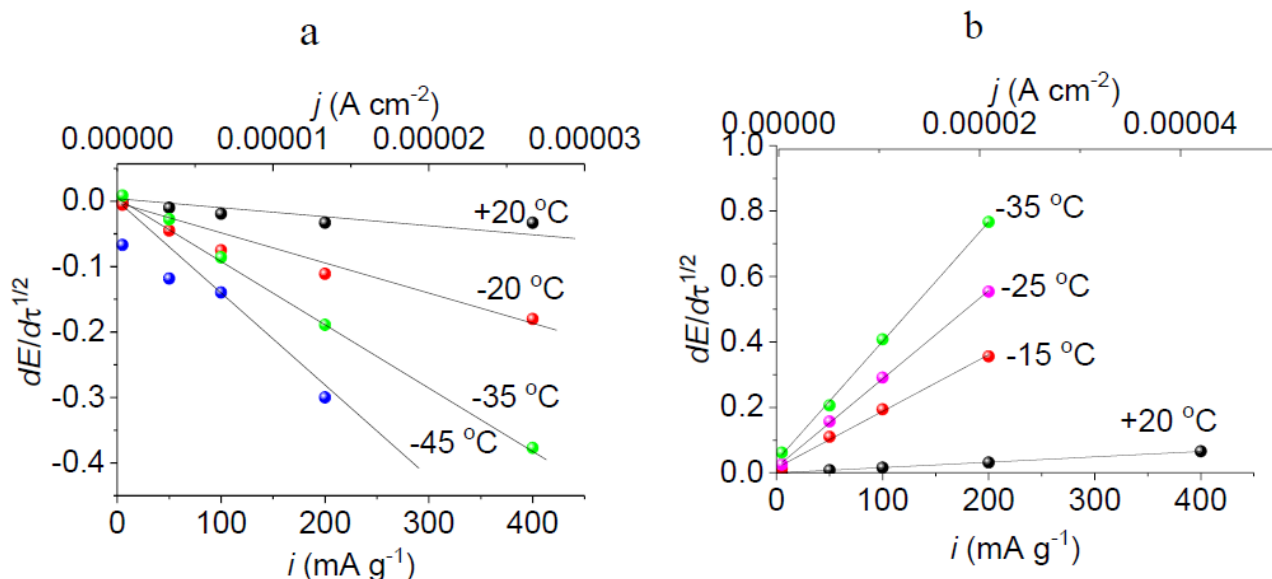


Figure 5. Dependences of $dE/d(\tau^{1/2})$ on the current density at different temperatures for $\text{Na}_3\text{V}_2(\text{PO}_4)_3@C$ (a) and $\text{Na}_2\text{Ti}_3\text{O}_7@C$ (b).

To calculate the effective diffusion coefficients of sodium (D_{eff}) in $\text{Na}_3\text{V}_2(\text{PO}_4)_3@C$ and $\text{Na}_2\text{Ti}_3\text{O}_7@C$, the formula [13, 14] was used:

$$D_{\text{eff}} = (4/n^2\rho^2\pi)(dE/dQ)^2/(d^2E/did(\tau^{1/2}))^2, \quad (6)$$

where ρ is the density of the active material and i is current density.

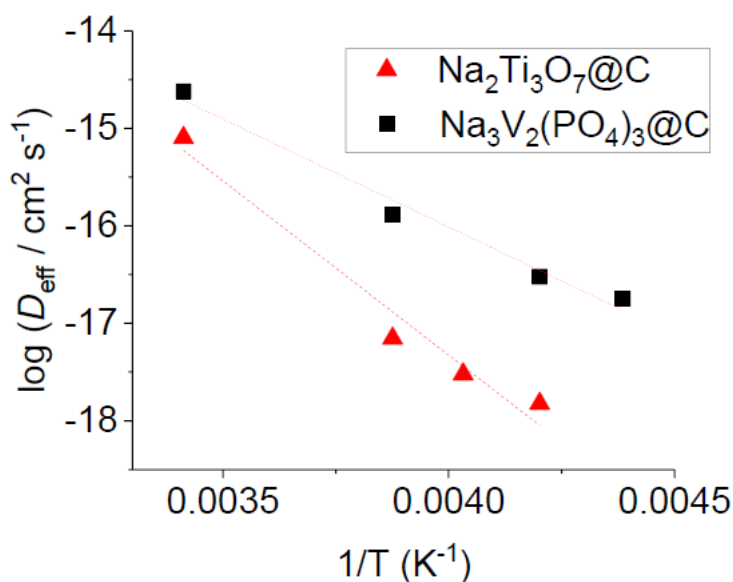
Formula (6) was derived based on solution of the second Fick's law with corresponding boundary condition in the limits of short times, and with due account for non-ideality of the system under consideration.

The values of dE/dQ were calculated from quasi-equilibrium curves of $\text{Na}_3\text{V}_2(\text{PO}_4)_3@C$ and $\text{Na}_2\text{Ti}_3\text{O}_7@C$. For $\text{Na}_3\text{V}_2(\text{PO}_4)_3@C$ and $\text{Na}_2\text{Ti}_3\text{O}_7@C$, these values were $1.37 \times 10^{-4} \text{ V g A}^{-1} \text{ s}^{-1}$ and $6.7 \times 10^{-5} \text{ V g A}^{-1} \text{ s}^{-1}$, respectively. The values of $d^2E/did(\tau^{1/2})$, as well as the calculated values of D_{eff} at different temperatures, are given in Table 1.

Table 1. The values of $d^2E/did(\tau^{1/2})$ and the calculated D_{eff} at different temperatures for $\text{Na}_3\text{V}_2(\text{PO}_4)_3@\text{C}$ and $\text{Na}_2\text{Ti}_3\text{O}_7@\text{C}$.

Temperature, °C	$d^2E/did(\tau^{1/2})$, Ohm $\text{cm}^2 \text{s}^{-1/2}$		D_{eff} , $\text{cm}^2 \text{s}^{-1}$	
	$\text{Na}_3\text{V}_2(\text{PO}_4)_3@\text{C}$	$\text{Na}_2\text{Ti}_3\text{O}_7@\text{C}$	$\text{Na}_3\text{V}_2(\text{PO}_4)_3@\text{C}$	$\text{Na}_2\text{Ti}_3\text{O}_7@\text{C}$
+20	1568	1517	2.4×10^{-15}	8×10^{-16}
-15	6766	16216	1.3×10^{-16}	7×10^{-18}
-25	-	24674	-	3×10^{-18}
-35	14356	34459	3×10^{-17}	1.5×10^{-18}
-45	21161		1.8×10^{-17}	

The dependence of the logarithm of the sodium diffusion coefficients in $\text{Na}_3\text{V}_2(\text{PO}_4)_3@\text{C}$ and $\text{Na}_2\text{Ti}_3\text{O}_7@\text{C}$ on the reciprocal absolute temperature is shown in Figure 6. These dependences are well described by the Arrhenius equation. The slopes are $2.2 \times 10^3 \text{ K}$ and $3.6 \times 10^3 \text{ K}$, which corresponds to the activation energy of sodium diffusion in $\text{Na}_3\text{V}_2(\text{PO}_4)_3@\text{C}$ and $\text{Na}_2\text{Ti}_3\text{O}_7@\text{C}$ as 43 and 70 kJ / mol, respectively.

**Figure 7.** Dependence of the logarithm of the diffusion coefficients of sodium in $\text{Na}_3\text{V}_2(\text{PO}_4)_3@\text{C}$ and $\text{Na}_2\text{Ti}_3\text{O}_7@\text{C}$ on the reciprocal absolute temperature.

Literary data on the activation energy of diffusion of sodium in a solid are extremely scarce. For example, in [15] the authors reported the results of a mathematical calculation of the activation energy of the diffusion of sodium ions in the four layered sodium transition metal oxides, NaMO_2 ($M = \text{V}, \text{Cr}, \text{Co}$ and Ni). In order of magnitude, the activation energy was 0.45 to 0.67 eV, which corresponds to 43–64 kJ / mol. The authors of [16], using impedance spectroscopy, determined the activation energy of diffusion of sodium ions in layered Na_xCoO_2 , depending on the degree of intercalation of sodium ions. Thus, with an intercalation degree equal to 0.5, the diffusion activation energy was 0.32 eV (30.7 kJ / mol), which in order agrees well with the results of our study.

5. CONCLUSIONS

In the present work, the performance of a sodium-ion battery based on sodium vanadium phosphate – sodium titanate in the temperature range from 20 to minus 45 °C was studied for the first time. It was established that the temperature dependence of the discharge capacity of the sodium-ion battery is determined by the temperature dependence of the discharge capacity of sodium titanate (negative electrode). The calculated values of the activation energy of sodium diffusion for sodium titanate and sodium vanadium phosphate were 42 and 70 kJ / mol, respectively. The increased value of the activation energy of sodium diffusion limits the functioning of sodium titanate at low temperatures.

ACKNOWLEDGEMENTS

The work was financially supported by the Russian Science Foundation (project 16-13-00024).

References

1. A. Ponrouch, M. R. Palacín, *Electrochem. Comm.*, 54 (2015) 51.
2. J.-Z. Guo, P.-F. Wang, X.-L. Wu, X.-H. Zhang, Q. Yan, H. Chen, J.-P. Zhang, Y.-G. Guo, *Adv. Mater.*, 29 (2017) 1701968.
3. Y. Huang, Y. Zheng, X. Li, F. Adams, W. Luo, Y. Huang, L. Hu, *ACS Energy Lett.*, 3 (2018) 1604.
4. Y. Wu, P. Nie, L. Wu, H. Dou, X. Zhang, *Chemical Engineering Journal*, 334, (2018) 932.
5. K.-C. Huang, J.-Z. Guo, H.-H. Li, H.-H. Fan, D.-H. Liu, Y.-P. Zheng, W.-L. Li, X.-L. Wu, J.-P. Zhang, *Journal of Alloys and Compounds*, 731 (2018) 881.
6. T. Liu, B. Wang, X. Gu, L. Wang, M. Ling, G. Liu, D. Wang, S. Zhang, *Nano Energy*, 30 (2016) 756.
7. K. Mukai, T. Inoue, Y. Kato, S. Shirai, *ACS Omega*, 2 (2017) 864.
8. A. Chekannikov, R. Kapaev, S. Novikova, N. Tabachkova, T. Kulova, A. Skundin, A. Yaroslavtsev, *J. Solid State Electrochem.*, 21 (2017) 1615.
9. L. Patterson, *Phys. Rev.*, 56 (1939) P. 978.
10. L. Si, Z. Yuan, L. Hu, Y. Zhu, Y. Qian, *J. Power Sources*, 272 (2014) 880.
11. I.-M. Hung, S. Jafian, N. V. Nghia, D.-L. Pham, *Ceramics International*, 43 (2017) S655.
12. Y. Zhang, H. Hou, X. Yang, J. Chen, M. Jing, Z. Wu, X. Jia, X. Ji, *J. Power Sources*, 305 (2016) 200.
13. T. L. Kulova, A. M. Skundin, E. A. Nizhnikovskii, A. V. Fesenko, *Russian Journal of Electrochemistry*, 42 (2006) 259.
14. T.L. Kulova, A.M. Skundin, *Russian Journal of Electrochemistry*, 42 (2006) 251.
15. G. Li, X. Yue, G. Luo, J. Zhao, *Computational Materials Science*, 106 (2015) 15.
16. T. Shibata, W. Kobayashi, Y. Moritomo, *Applied Physics Express*, 6 (2013) 097101.